# The Bone Sialoprotein RGD Domain Modulates and Maintains Periodontal Development

Journal of Dental Research
2022, Vol. 101(10) 1238–1247

DOI: 10.1177/00220345221100794
journals.sagepub.com/home/jdr

**K. Nagasaki[1], M.B. Chavez[2], A. Nagasaki[1], J.M. Taylor[1], M.H. Tan[2], M. Ma[1], E. Ralston[3], M.E. Thew[4], D.-G. Kim[4], M.J. Somerman[1], and B.L. Foster[2]**

**Abstract**

Bone sialoprotein (gene: *Ibsp*; protein: BSP) is a multifunctional extracellular matrix protein present in bone, cementum, and dentin. Accumulating evidence supports BSP as a key regulator of mineralized tissue formation via evolutionarily conserved functional domains, including a C-terminal integrin-binding Arg-Gly-Asp (RGD) domain implicated in extracellular matrix–cell signaling. Ablation of *Ibsp* in mice ($Ibsp^{-/-}$) results in impaired bone growth and mineralization and defective osteoclastogenesis, with effects in the craniofacial region including reduced acellular cementum formation, detachment of the periodontal ligament (PDL), alveolar bone hypomineralization, and severe periodontal breakdown. We hypothesized that BSP-RGD plays an important role in cementum and alveolar bone formation and mineralization, as well as periodontal function. This hypothesis was tested by replacing the RGD motif with a nonfunctional Lys-Ala-Glu (KAE) sequence in ($Ibsp^{KAE/KAE}$) mice and OCCM.30 murine ($Ibsp^{KAE}$) cementoblasts. The RGD domain was not critical for acellular or cellular cementum formation in $Ibsp^{KAE/KAE}$ mice. However, PDL volume and thickness were increased, and significantly more tartrate-resistant acid phosphatase–positive osteoclasts were found on alveolar bone surfaces of $Ibsp^{KAE/KAE}$ mice versus wild type mice. PDL organization was disrupted as indicated by picrosirius red stain, second harmonic generation imaging, dynamic mechanical analysis, and decreased asporin proteoglycan localization. In vitro studies implicated RGD functions in cell migration, adhesion, and mineralization, and this was confirmed by an ossicle implant model where cells lacking BSP-RGD showed substantial defects as compared with controls. In total, the BSP-RGD domain is implicated in periodontal development, though the scale and scope of changes indicated by in vitro studies indicate that other factors may partially compensate for and reduce the phenotypic severity of mice lacking BSP-RGD in vivo.

**Keywords:** periodontium, extracellular matrix, biomineralization, dental cementum, bone, integrins

## Introduction

Bone sialoprotein (gene: *Ibsp*; protein: BSP) is a multifunctional extracellular matrix (ECM) protein of the SIBLING family (small integrin-binding ligand N-linked glycoprotein) present in bone, cementum, and dentin (Ganss et al. 1999; Fisher and Fedarko 2003). Accumulating evidence supports BSP as a key regulator of mineralized tissue formation via evolutionarily conserved functional domains, including an N-terminal collagen-binding domain, polyglutamic (polyE) acid sequences that nucleate hydroxyapatite, and a C-terminal integrin-binding Arg-Gly-Asp (RGD) domain. In BSP, the RGD domain mediates cell attachment and migration via $\alpha_v\beta_3$ and $\alpha_v\beta_5$ integrins (Bellahcène et al. 2000; Rapuano et al. 2004; Karadag and Fisher 2006) and modulates osteoblast/osteoclast formation and activity via $\alpha_v\beta_3$ and the FAK-MAPK (focal adhesion kinase–mitogen-activated protein kinase) signaling pathway (Valverde et al. 2005; Gordon et al. 2009). However, studies on the BSP-RGD domain have been limited to in vitro assays, emphasizing the need for in vivo experiments to investigate physiologic functions.

Ablation of *Ibsp* in mice ($Ibsp^{-/-}$) impairs long bone growth and mineralization and osteoclastogenesis (Malaval et al. 2008; Holm et al. 2015). Yet, BSP plays arguably more critical roles in the craniofacial region. As an ECM protein linked to differentiation of cementoblasts and osteoblasts and mineralization of cementum and alveolar bone, BSP is positioned to play important functions in preserving the periodontal complex. $Ibsp^{-/-}$ mice exhibit reduced acellular cementum formation,

[1]Laboratory of Oral Connective Tissue Biology, National Institute of Arthritis and Musculoskeletal and Skin Diseases, National Institutes of Health, Bethesda, MD, USA
[2]Biosciences Division, College of Dentistry, The Ohio State University, Columbus, OH, USA
[3]Light Imaging Section, Office of Science and Technology, National Institute of Arthritis and Musculoskeletal and Skin Diseases, National Institutes of Health, Bethesda, MD, USA
[4]Division of Orthodontics, College of Dentistry, The Ohio State University, Columbus, OH, USA

A supplemental appendix to this article is available online.

**Corresponding Author:**
B.L. Foster, Biosciences Division, College of Dentistry, The Ohio State University, 4163 Postle Hall, 305 W 12th Avenue, Columbus, OH 43210, USA.
Email: foster.1004@osu.edu

detachment of the periodontal ligament (PDL), alveolar bone hypomineralization, and severe periodontal breakdown (Foster et al. 2013, 2015; Soenjaya et al. 2015). The mechanisms underlying these dentoalveolar defects remain unclear, in part because the respective contributions of BSP domains remain uncertain.

To test the importance of the BSP-RGD domain in dentoalveolar development and function, the RGD motif was replaced by a nonfunctional Lys-Ala-Glu (KAE) sequence (Bellahcène et al. 2000; Gordon et al. 2009) in mice and OCCM.30 cementoblasts. We hypothesized that BSP-RGD functions in cell-ECM interactions were important in cementum and alveolar bone formation and function.

## Materials and Methods

### Mice

Animal studies were approved by the Animal Care and Use Committee (National Institutes of Health). Previous analyses of *Ibsp*$^{-/-}$ mice used a 129/CD1 mouse genetic background (Malaval et al. 2008; Foster et al. 2013, 2015). The majority of new genetically engineered mouse models are prepared on an inbred standardized C57BL/6 background (Appendix); therefore, *Ibsp*$^{-/-}$ mice on a C57BL/6 genetic background were engineered (Appendix Fig. 1). For continuity, these mice and appropriate wild type (WT) controls were compared with previously described *Ibsp*$^{-/-}$ mice on a 129/CD1 background (Foster et al. 2013, 2015). *Ibsp*$^{KAE/KAE}$ mice were generated on a C57BL/6 background by CRISPR/Cas9 gene editing to replace the RGD domain of BSP with a nonfunctional KAE sequence (Appendix Fig. 2). New mouse models were generated by Taconic Biosciences and sequenced to confirm deletion/substitution. Mice were euthanized, and mandibles were harvested at 10 d postnatal (dpn; active *Ibsp* mRNA expression in cementoblasts and alveolar bone osteoblasts), 14 dpn (prior to molar eruption), 26 dpn (shortly after first molar eruption), and 60 dpn (>1 mo occlusion). *Ibsp* mRNA was analyzed at 10 dpn, an active period of periodontal development when cementoblasts and osteoblasts highly express *Ibsp* (MacNeil et al. 1995). Additional details are in the Appendix.

### Micro–computed tomography

Hemimandibles for micro–computed tomography were fixed in 10% neutral buffered formalin ($n$ = 3 to 8/genotype), scanned in a μCT 50 scanner (Scanco Medical), and analyzed as previously described (Chavez et al. 2021). Additional details are in the Appendix.

### Histology

Hemimandibles for histology were fixed in Bouin's solution for 24 h, decalcified in an acetic acid–formalin–sodium chloride solution, and paraffin embedded for serial 5-μm coronal sections (Foster et al. 2015). Hematoxylin and eosin, tartrate-resistant acid phosphatase (TRAP), picrosirius red, immunohistochemistry, and in situ hybridization stains ($n$ = 3 to 5/genotype) were described previously (Foster et al. 2018).

### Second Harmonic Generation Microscopy

Hemimandibles for second harmonic generation ($n$ = 3/genotype) were fixed in 2% paraformaldehyde and 2% glutaraldehyde in phosphate buffer for 24 h and plastic embedded for sawing to the first molar mesial root by a low-speed diamond saw (Bueheler; Naveh et al. 2018). Additional details are in the Appendix.

### Dynamic Mechanical Analysis

Unfixed hemimandibles (26 dpn; $n$ = 6 or 7/genotype) underwent dynamic mechanical analysis to measure static stiffness (K), hysteresis (W), dynamic stiffness (K*), elastic stiffness (K′), loss stiffness (K″), and energy dissipation (tan δ), as previously described (Zhang et al. 2020). Additional details are in the Appendix.

### Cell Culture

A homozygous *Ibsp* knock-in cementoblast cell line (*Ibsp*$^{KAE}$), where the RGD motif was replaced by a nonfunctional sequence, was generated from the well-established immortalized murine cementoblasts (OCCM.30) as a WT parent strain (D'Errico et al. 1999) with CRISPR/Cas9 at the Transgenic Core Facility (National Heart, Lung, and Blood Institute, National Institutes of Health). *Ibsp* knockout cells (*Ibsp*$^{\Delta Nterm}$; Ao et al. 2017) were used as a comparison. Additional details are in the Appendix and in Appendix Figure 3. Migration, adhesion, and mineralization assays are detailed in the Appendix and in Appendix Figure 4.

### Ossicle Implant Model

An ossicle implant model tested the ability of cells to promote in vivo mineral nodule formation (Ao et al. 2017) in collagen-elastin sponges implanted subcutaneously in SCID mice (NOD.Cg-Prkdc$^{scid}$Il2rg$^{tm1Wjl}$/SzJ; $n$ = 4/genotype). Additional details are in the Appendix.

### Statistical Analysis

Results are expressed as mean ± standard deviation. Data were analyzed with $t$ test for independent samples or 1-way analysis of variance with post hoc Tukey test (Prism 7.04; GraphPad Software). For all tests, $\alpha = 0.05$.

## Results

### Altered Periodontal Structures in the Absence of the BSP-RGD Motif

Previous data on global BSP ablation used *Ibsp*$^{-/-}$ mice on a mixed 129/CD1 genetic background (Malaval et al. 2008; Foster et al. 2013, 2015). *Ibsp*$^{-/-}$ and *Ibsp*$^{KAE/KAE}$ mice described here were generated on a C57BL/6 genetic background to provide an established inbred mouse model. Given reports that genetic background affects mouse phenotypes (Iwaniec et al.

2006; Mukhopadhyay et al. 2012) and prior to focused studies on the role of the BSP-RGD motif in modulating the periodontia, we comparatively analyzed the dental and periodontal effects of *Ibsp* knockout on both genetic backgrounds at 60 dpn. In brief, when compared with WT controls, $Ibsp^{-/-}$ mice on a C57BL/6 background exhibited reduced acellular cementum and PDL detachment, significantly reduced alveolar bone proper (ABP) volume, and incisor alterations associated with defective eruption, but they had an overall milder mineralization phenotype than $Ibsp^{-/-}$ mice on a 129/CD1 background. Additional details are in the Appendix and in Appendix Figures 5 and 6.

To define the functions of the BSP-RGD motif, we genetically edited the RGD domain to be replaced by the nonfunctional KAE motif and analyzed homozygous $Ibsp^{KAE/KAE}$ mice on the C57BL/6 background. No differences were found in enamel or dentin/cementum volumes or densities by micro–computed tomography analyses of molars in $Ibsp^{KAE/KAE}$ versus WT mice at 14, 26, or 60 dpn (Appendix Fig. 7). In periodontal tissues, mandibular bone and ABP volume and density were not altered in $Ibsp^{KAE/KAE}$ mice (Fig. 1A–E). However, PDL volume was significantly increased in $Ibsp^{KAE/KAE}$ versus WT at 26 and 60 dpn (10% and 18%, respectively; $P < 0.01$ and $P < 0.001$), mirrored by 20% increased PDL thickness at 60 dpn ($P < 0.05$). Notably, $Ibsp^{KAE/KAE}$ mice did not share incisor alterations with $Ibsp^{-/-}$ mice, with a 5% reduction in incisor volume ($P < 0.01$) and 85% reduction in incisor pulp volume ($P < 0.0001$; Appendix Fig. 5), but rather showed normal overall volume and pulp volume at 60 dpn (Fig. 1F).

In situ hybridization at 10 dpn during active periodontal formation indicated unchanged numbers and density of $Ibsp^{+}$ cementoblasts on root surfaces and osteoblasts on alveolar bone surfaces (Fig. 2A–C). Immunohistochemistry at 60 dpn confirmed normal localization of BSP in mature and functional cementum and alveolar bone of $Ibsp^{KAE/KAE}$ versus WT mice (Fig. 2D). Histology showed normal tissue morphology, including no acellular or cellular cementum defects and normal PDL attachment in $Ibsp^{KAE/KAE}$ mice (Fig. 2E–H).

Altered PDL volume and thickness in $Ibsp^{KAE/KAE}$ mice prompted us to analyze tissues for the presence of $TRAP^{+}$ osteoclast-like cells that may promote alveolar bone resorption. TRAP staining revealed a 60% to 180% increase in osteoclast cell density on the alveolar bone surfaces of $Ibsp^{KAE/KAE}$ versus WT mice at 14 ($P < 0.05$), 26 ($P < 0.01$), and 60 dpn ($P < 0.01$; Fig. 2I, J). Osteoclast/odontoclast cells were not observed along tooth root surfaces from $Ibsp^{KAE/KAE}$ or WT mice.

## Altered PDL Structure and Mechanical Properties in the Absence of the BSP-RGD Motif

Altered PDL parameters in $Ibsp^{KAE/KAE}$ mice prompted further analysis of the PDL region. When compared with WT well-organized PDL collagen fibers, with insertion of Sharpey's fibers into cementum, $Ibsp^{KAE/KAE}$ mice had disorganized PDL fiber orientation at 14, 26, and 60 dpn (Fig. 3A). Second harmonic generation microscopy, used to image fibrillar collagen under confocal microscopy, revealed highly organized PDL collagen fibrils (green signal) in 26-dpn WT, while $Ibsp^{KAE/KAE}$ tissues displayed relatively thin, sparse, and disoriented fibrils (Fig. 3B).

Immunohistochemistry for a panel of PDL protein and proteoglycan markers revealed decreased staining for asporin within the PDL, with slightly higher expression near the root, in $Ibsp^{KAE/KAE}$ versus WT at 26 and 60 dpn (Fig. 3C). Localization and abundance of decorin, lumican, biglycan, and periostin appeared unchanged in $Ibsp^{KAE/KAE}$ versus WT periodontal tissues (Appendix Fig. 8).

Given the altered structure and composition of $Ibsp^{KAE/KAE}$ versus WT periodontal tissues, we performed dynamic mechanical analysis to test mechanical properties of the PDL. When compared with WT, $Ibsp^{KAE/KAE}$ mice exhibited significantly lower dynamic stiffness (K*) and elastic (storage) stiffness (K′; $P < 0.05$ for both), while other dynamic mechanical analysis parameters were not significantly different (Fig. 3D).

## The RGD Domain of BSP Regulates In Vitro Cell Migration, Adhesion, and Ossicle Mineralization

Altered PDL structure, composition, and mechanical properties associated with lack of the BSP-RGD motif prompted us to investigate in vitro cell functions. $Ibsp^{KAE}$ OCCM.30 immortalized murine cementoblasts carrying the inactivating RGD mutation were compared with previously described OCCM.30 cells harboring a large N-terminal deletion ($Ibsp^{\Delta Nterm}$; Ao et al. 2017). While no changes were noted in cell proliferation at 24 h between cell types, $Ibsp^{KAE}$ and $Ibsp^{\Delta Nterm}$ cementoblasts exhibited a 30% to 40% reduced migration rate, with no significant difference between them, as compared with WT cells (Fig. 4A, B).

The ability of cells to adhere to dishes precoated with the RGD motif–containing ECM protein, fibronectin (FN) indicated that $Ibsp^{KAE}$ and $Ibsp^{\Delta Nterm}$ cells had greater sensitivity to and increased adherence on FN versus WT cells (Fig. 4C). Because of differences in cell-ECM adhesion to FN, cells were tested on dishes precoated with recombinant BSP (rBSP), rBSP-KAE, or RGD peptide. WT, $Ibsp^{KAE}$, and $Ibsp^{\Delta Nterm}$ cells all showed significantly less adhesion to rBSP(KAE) versus rBSP(RGD; $P < 0.0001$ for all comparisons). All cells showed relatively greater adhesion to RGD versus rBSP(KAE), though $Ibsp^{KAE}$ showed the greatest sensitivity and response versus the other cell types (Fig. 4D).

$Ibsp^{KAE}$ cells promoted mineral nodule formation equivalent to WT cells, while $Ibsp^{\Delta Nterm}$ cells exhibited 70% reduced mineralization capacity by alizarin red staining (Fig. 4E, F). The in vivo ossicle implant model revealed that $Ibsp^{KAE}$ and $Ibsp^{\Delta Nterm}$ cells produced smaller ossicles versus WT cells ($P < 0.0001$; Fig. 4G). No differences were detected between $Ibsp^{KAE}$ and $Ibsp^{\Delta Nterm}$ implants. Negative controls (no cells) exhibited minimal volume and mineral density. Hematoxylin and eosin staining of decalcified nodules showed similar distribution of cells and ECM in WT and $Ibsp^{KAE}$ cementoblasts, while $Ibsp^{\Delta Nterm}$ cells were present in a matrix appearing like osteoid/cementoid, as previously described (Ao et al. 2017).

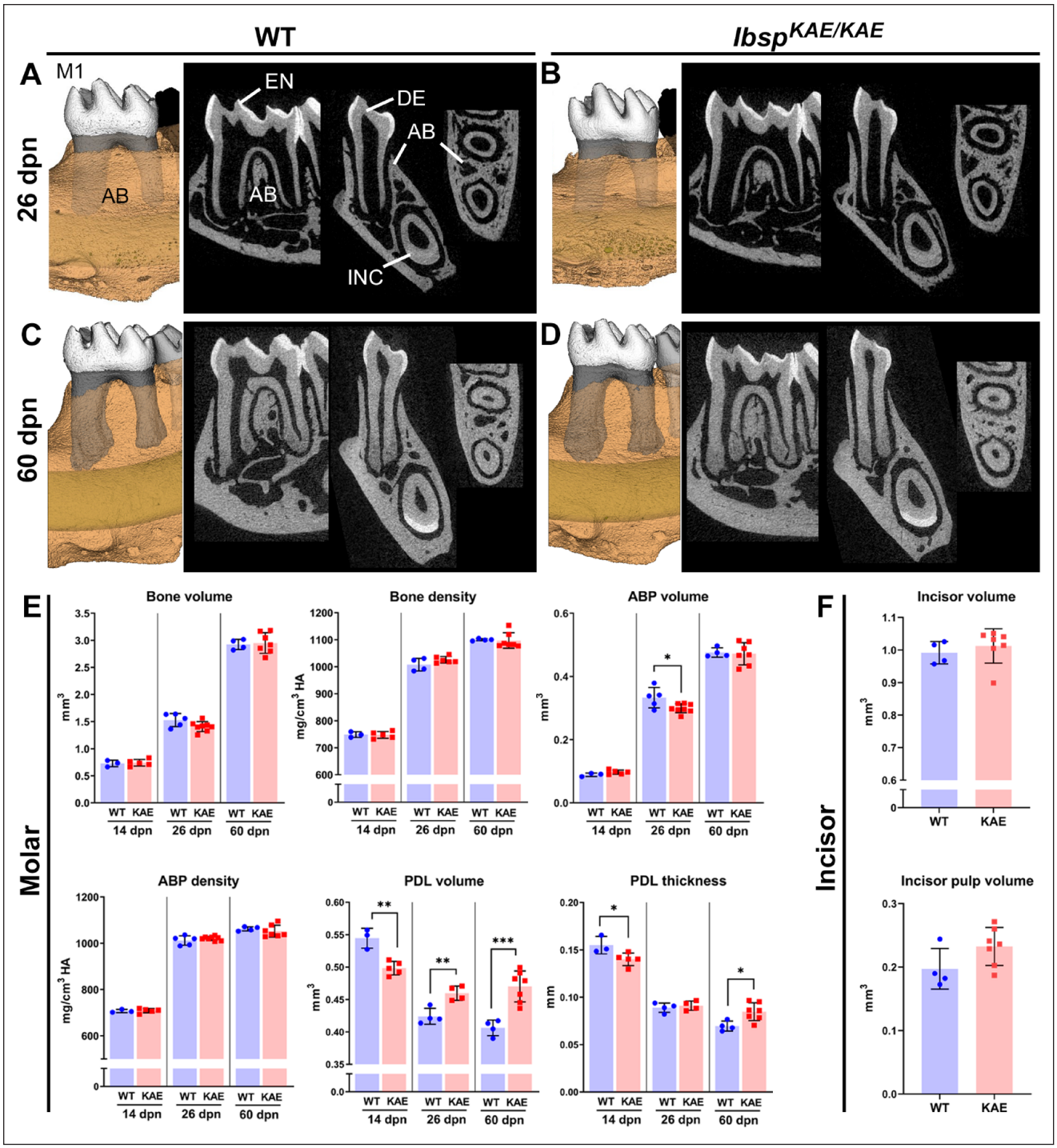


**Figure 1.** Altered periodontal structures in the absence of the BSP-RGD motif. (**A–D**) Representative 3- and 2-dimensional micro–computed tomography renderings of first mandibular molars (M1) from wild type (WT) and *Ibsp*$^{KAE/KAE}$ mice on a C57BL/6 genetic background at 26 and 60 dpn (days postnatal). There are no obvious differences in enamel (EN), dentin (DE), alveolar bone (AB), or incisor (INC) tissues. (**E**) Quantitative measurements from 14, 26, and 60 dpn reveal transiently reduced alveolar bone proper (ABP) in *Ibsp*$^{KAE/KAE}$ versus WT mice at 26 dpn ($n$ = 3 to 7/genotype/age). When compared with WT, *Ibsp*$^{-/-}$ mice have persistently altered periodontal ligament (PDL) volume and thickness (first decreased, then increased). (**F**) INC volume and INC pulp volume was not different between genotypes. Mean ± SD. *$P$ < 0.05. **$P$ < 0.01. ***$P$ < 0.001.

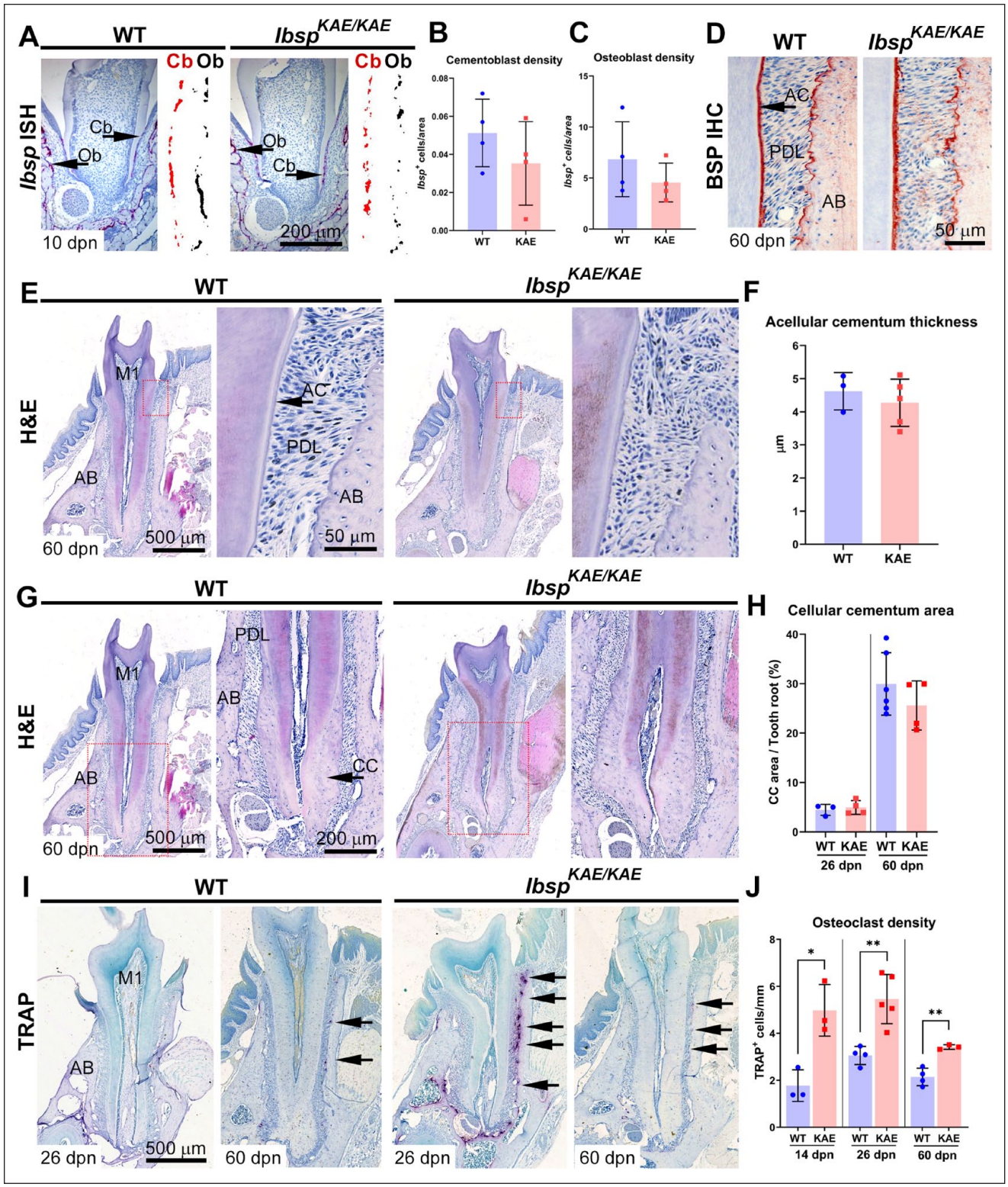


**Figure 2.** Normal cementum development but increased osteoclast numbers in the absence of BSP-RGD. (**A**) In situ hybridization (ISH) for *Ibsp* mRNA at 10 dpn (days postnatal) indicates a similar distribution of *Ibsp*$^{+}$ cementoblasts (Cb) at root surfaces and osteoblasts (Ob) on alveolar bone surfaces of *Ibsp*$^{KAE/KAE}$ versus wild type (WT) mice, confirmed by (**B**, **C**) cell density calculations ($n$ = 4/genotype). (**D**) Immunohistochemistry (IHC) shows normal distribution of BSP in acellular cementum (AC) and alveolar bone (AB). PDL, periodontal ligament. (**E**) Histology at 60 dpn illustrates normal dentoalveolar tissue morphology and no PDL detachment in *Ibsp*$^{KAE/KAE}$ mice. H&E, hematoxylin and eosin; M1, first mandibular molar. (**F**) Histomorphometry demonstrates normal AC thickness in *Ibsp*$^{KAE/KAE}$ versus WT mice at 60 dpn ($n$ = 3 to 5/genotype). (**G**) Histology at 60 dpn indicates normal cellular cementum (CC) formation, confirmed by (**H**) histomorphometry ($n$ = 3 to 5/genotype). (**I**, **J**) TRAP staining reveals increased densities of TRAP$^{+}$ osteoclast-like cells (stained red, indicated by black arrows) on *Ibsp*$^{KAE/KAE}$ versus WT AB surfaces at 14, 26, and 60 dpn ($n$ = 3 to 5/genotype/age). Mean ± SD. *$P < 0.05$. **$P < 0.01$.

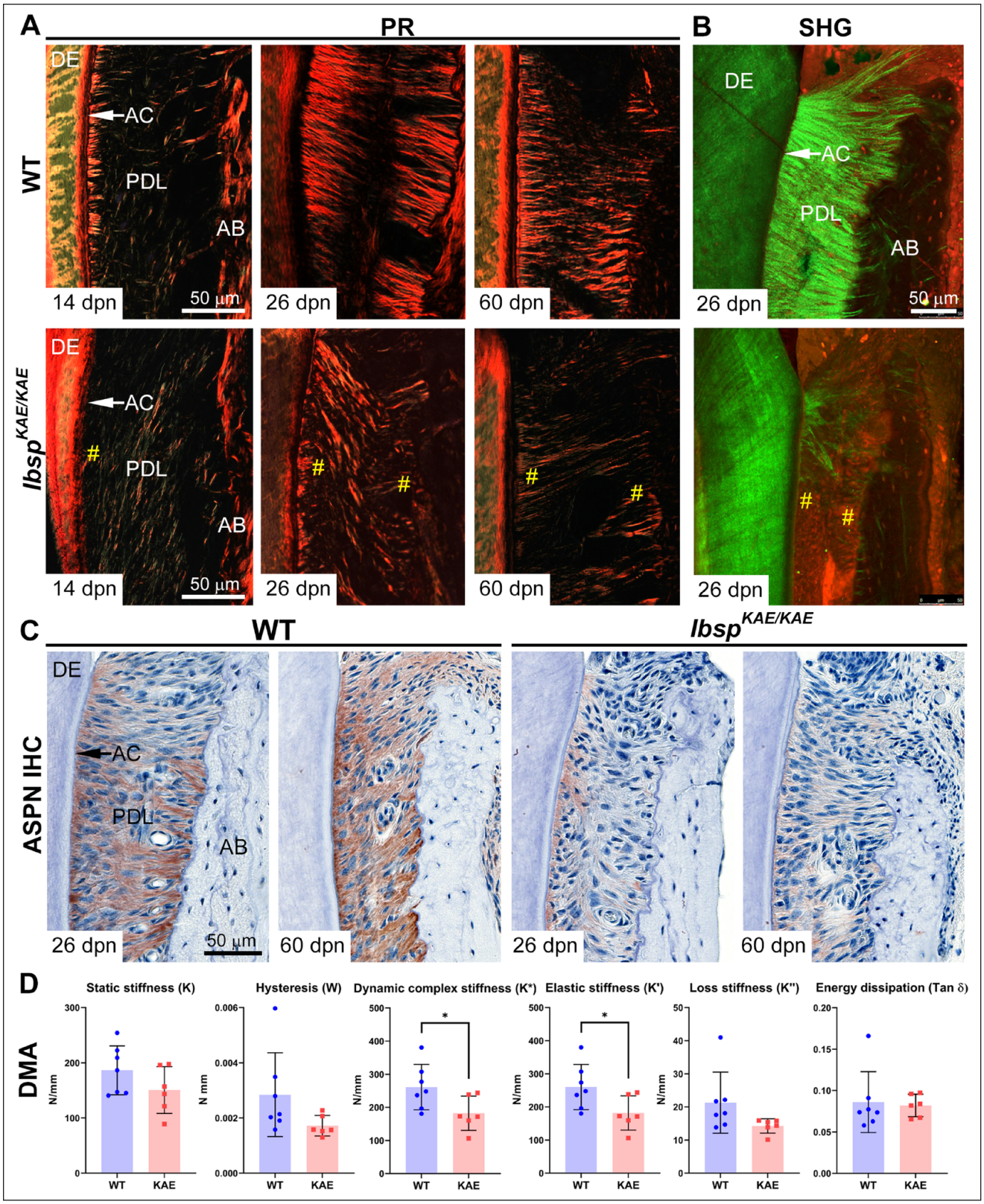


**Figure 3.** Altered periodontal ligament (PDL) structure and mechanical properties in the absence of the BSP-RGD motif. (**A**) By picrosirius red (PR) staining, *Ibsp*$^{KAE/KAE}$ mice show disorganized PDL fiber orientation versus wild type (WT) mice at 14, 26, and 60 dpn (days postnatal; $n = 3$ to 5/genotype). (**B**) Second harmonic generation (SHG) microscopy demonstrates highly organized PDL collagen fibrils in WT at 26 dpn (green signal), while *Ibsp*$^{KAE/KAE}$ tissues reveal relatively thin, sparse, and disoriented fibrils ($n = 3$/genotype). (**C**) Immunohistochemistry (IHC) illustrates decreased staining for asporin (ASPN) in *Ibsp*$^{KAE/KAE}$ versus WT PDL at 26 and 60 dpn ($n = 3$ to 5/genotype). (**D**) Dynamic mechanical analysis (DMA) reveals that *Ibsp*$^{KAE/KAE}$ mice exhibit lower values for dynamic stiffness (K*) and elastic (storage) stiffness (K′) when compared with WT at 26 dpn ($n = 6$/genotype). AB, alveolar bone; AC, acellular cementum; DE, dentin. Mean ± SD. *$P < 0.05$.

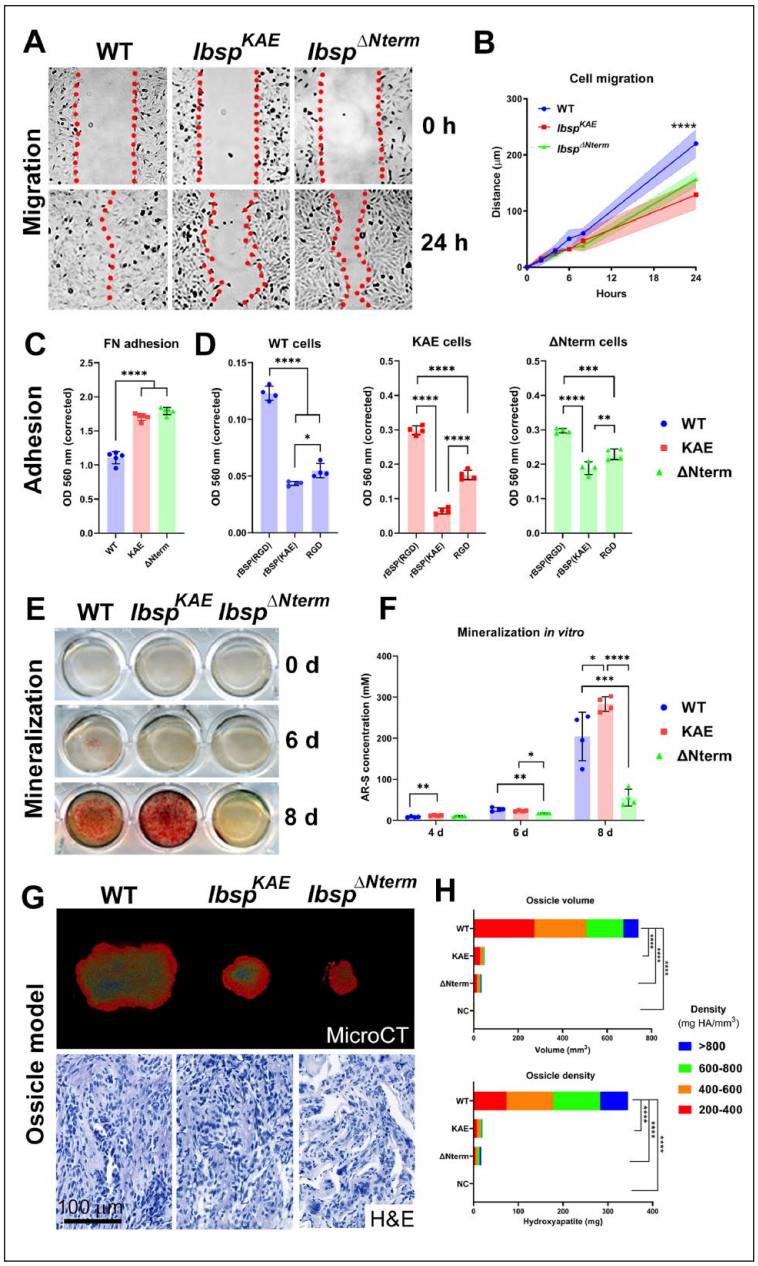


**Figure 4.** The RGD domain of BSP regulates in vitro cell migration and adhesion and in vivo mineralization. *Ibsp*$^{KAE}$ OCCM.30 immortalized murine cementoblasts carrying the inactivating RGD mutation were compared to wild type (WT) cells and cells harboring a large N-terminal deletion (*Ibsp*$^{\Delta Nterm}$). (**A**, **B**) When compared with WT cells, *Ibsp*$^{KAE}$ and *Ibsp*$^{\Delta Nterm}$ cementoblasts exhibit a reduced migration rate by 24 h, with no difference between them. (**C**) The KAE or ΔNterm mutations cause increased OCCM.30 cell adhesion to fibronectin (FN) ($n$ = 5/genotype). (**D**) WT, *Ibsp*$^{KAE}$, and *Ibsp*$^{\Delta Nterm}$ cells all show reduced adhesion to rBSP(KAE) versus rBSP(RGD). All cells have relatively greater adhesion to RGD versus rBSP(KAE), though *Ibsp*$^{KAE}$ has the greatest sensitivity and response versus the other cell types ($n$ = 4/genotype). (**E**, **F**) Under in vitro mineralization conditions, *Ibsp*$^{KAE}$ cells promote mineral nodule formation equivalent to WT cells, while *Ibsp*$^{\Delta Nterm}$ cells exhibit reduced mineralization capacity by alizarin red staining. (**G**) When compared with large mineralized ossicles produced by WT OCCM.30 cells in vivo, *Ibsp*$^{KAE}$ and *Ibsp*$^{\Delta Nterm}$ cells produce smaller ossicles ($n$ = 4/genotype). Hematoxylin and eosin (H&E) staining shows similar distribution of cells and extracellular matrix in WT and *Ibsp*$^{KAE}$ cementoblasts, while *Ibsp*$^{\Delta Nterm}$ cells are present in a matrix appearing like osteoid/cementoid. (**H**) Quantitative analysis demonstrates greater ossicle volume and mineral density by WT cells, with no differences between *Ibsp*$^{KAE}$ and *Ibsp*$^{\Delta Nterm}$ cells. Key for mineral density: red, 200 to 400 mg/cm$^3$ hydroxyapatite (HA); orange, 400 to 600 mg/cm$^3$ HA; green, 600 to 800 mg/cm$^3$ HA; blue, > 800 mg/cm$^3$ HA. Mean ± SD. *$P$ < 0.05. **$P$ < 0.01. ***$P$ < 0.001. ****$P$ < 0.0001.

## Discussion

BSP plays a key role in bone homeostasis and is essential for cementum formation and periodontal function. We examined the functional importance of the BSP-RGD domain with multimodal in vivo and in vitro approaches, replacing RGD with a nonfunctional KAE sequence. While the RGD domain was not critical for cementum or alveolar bone mineralization, periodontal structure, organization, composition, and function were affected in mice (Appendix Tables 1 and 2). In vitro studies implicated RGD functions in cell migration, adhesion, and mineralization, as confirmed by an ossicle implant model where cells lacking BSP-RGD showed substantially defective mineralization versus controls. In total, the BSP-RGD domain is implicated in periodontal development, though in vitro studies indicate that other factors may partially compensate for and reduce the phenotypic severity of mice lacking BSP-RGD.

### *Functions of the BSP-RGD Motif in Dentoalveolar Development*

The most striking dentoalveolar effect of global BSP knockout in mice is the lack of functional acellular cementum, causing PDL detachment and severe periodontal breakdown, also contributing to incisor malocclusion in mice on a 129/CD1 background (Foster et al. 2013, 2015; Soenjaya et al. 2015) and with a milder phenotype on the C57BL/6 background analyzed here. Key initial findings in mice lacking the BSP-RGD domain were presence of acellular cementum, with no observed PDL detachment, periodontal destruction, or incisor malocclusion. These collective observations suggest that RGD-associated functions are not responsible for the major cementum and alveolar bone hypomineralization phenotypes arising from BSP ablation, thereby pointing to other BSP domains, including the N-terminal hydrophobic collagen-binding motif and polyE mineral-nucleating sequences, with additional potential contributions from phosphorylated serines and glycosylation (Tye et al. 2005; Xu et al. 2017).

While a cementum phenotype was not identified, these studies revealed a vital role for BSP-RGD in periodontal tissues by multiple lines of evidence. As a marker for cementoblasts and osteoblasts contributing to cell differentiation and tissue mineralization, BSP is positioned to function in PDL attachment and periodontal integrity. However, it was surprising that primary changes were detected in PDL organization and composition, rather than in cementum and bone. Analyses revealed decreased PDL volume and thickness prior to tooth eruption in the absence of BSP-RGD. While root formation,

alveolar bone remodeling, and organization of the PDL from the dental follicle are understood to be intimately connected developmental processes (Radlanski et al. 2015), little is known about cellular regulators—for example, how dental follicle cell fates are determined to contribute to cementoblasts, PDL fibroblasts, or alveolar bone osteoblasts. These early PDL differences may reflect altered differentiation, migration, and/or accumulation of dental follicle cells to root and/or bone surfaces. Conversely, we found increased PDL parameters at later ages and decreased ABP in the absence of BSP-RGD. Increased numbers of osteoclasts were present on alveolar bone surfaces of $Ibsp^{KAE/KAE}$ versus WT mice, and osteoclast resorption likely contributes to the observed PDL and ABP changes. Though the PDL was structurally altered, $Ibsp^{KAE/KAE}$ maintained periodontal attachment, structure, and function, within the limits of this study. $Ibsp^{-/-}$ and $Ibsp^{KAE/KAE}$ mice share the presence of increased numbers of osteoclasts on alveolar bone, but they differ in that $Ibsp^{-/-}$ mice demonstrate reduced osteoclast differentiation and function in long bones (Malaval et al. 2008; Boudiffa et al. 2010), with evidence that BSP contributes to osteoclast differentiation in vitro (Valverde et al. 2005) and in vivo (Valverde et al. 2008). We hypothesize that altered periodontal structures in mice with BSP knockout or RGD mutation attract and activate more osteoclast precursors, overriding inherent cell-autonomous functional defects. While at later ages, altered periodontal structures in $Ibsp^{KAE/KAE}$ mice might be a factor in attraction of osteoclasts, increased osteoclast numbers even at 14 dpn, prior to molar eruption, suggest that altered occlusal forces are not primarily responsible. Work is ongoing to analyze the skeletal phenotype of the $Ibsp^{KAE/KAE}$ mice and investigate effects on osteoclastogenesis in vitro.

Picrosirius red stain and second harmonic generation microscopy revealed reduced organization of PDL in $Ibsp^{KAE/KAE}$ mice versus controls. Mechanical testing revealed differences at a posteruption age, with lower dynamic and storage stiffness reflecting PDL changes, with additional contributions from disordered PDL organization. Though $Ibsp^{KAE/KAE}$ teeth show more displacement under loading, they still bear chewing forces and maintain energy dissipation comparable to WT.

Previous studies have highlighted the importance of small leucine-rich proteoglycans (SLRPs) in PDL function and collagen organization, affecting cell mechanosensory functions. Mice genetically ablated for SLRP fibromodulin and biglycan exhibited disrupted PDL collagen fibrillogenesis, overexpression of asporin, hyperactive TGFβ/BMP signaling, and increased numbers of osteoclasts on alveolar bone (Wang et al. 2014). In our studies we noted decreased expression of asporin in $Ibsp^{KAE/KAE}$ mice versus WT mice in a gradient fashion, with greater localization in proximity to the root surface, while the other SLRPs and periostin were unaltered. Asporin was reported to be a negative regulator of mineralization when overexpressed in PDL cells (Kajikawa et al. 2014), while conflicting reports indicate a positive effect on mineralization (Lee et al. 2011; Xu et al. 2015; Zhan et al. 2019). Asporin overexpression/treatment in fibroblasts was shown to increase collagen calcification and prevent mechanosensory-induced ECM remodeling (Liu et al. 2021). These accumulated findings indicate a role for asporin in cell-ECM interactions, including within the periodontal complex, though further studies are required.

## *The RGD Domain of BSP Controls Migration and Adhesion of Cementoblasts In Vitro*

Periodontal alterations in mice lacking BSP-RGD prompted us to explore functions of the domain in vitro. We mutated BSP-RGD to KAE via CRISPR/Cas9 in a well-established immortalized cementoblast cell line, OCCM.30 cells (D'Errico et al. 1999), comparing them with WT OCCM.30 cells and $Ibsp^{\Delta Nterm}$ cells featuring a large N-terminal deletion (Ao et al. 2017). Migration and adhesion assays revealed a marked effect of the absence of the RGD domain, suggesting key roles for this domain in cell interactions with the surrounding ECM and environment. $Ibsp^{\mathrm{KAE}}$ cells showed increased adhesion to FN and a hypersensitive response to RGD versus rBSP(KAE). Other conserved motifs in BSP are known to be involved in cell-ECM interactions, most notably the collagen-binding domain (Tye et al. 2005), and $Ibsp^{\Delta Nterm}$ cells (lacking that domain an additional N-terminal residues) showed altered adhesion to all ECM proteins tested.

$Ibsp^{KAE}$ cementoblast mineralization appeared undiminished when compared with WT by alizarin red staining, supporting the BSP polyE domains (and possibly other regions) as the primary modulators of mineralization (Goldberg et al. 2001). However, the ossicle implant model indicted severe defects in $Ibsp^{KAE}$ cells, reflected as reduced ossicle volume and hydroxyapatite deposition. Considering the combined in vivo and in vitro data, these contrasting results do not appear to be from impaired mineralization per se but may implicate altered cell-ECM interactions, such as those highlighted by impaired migration and adhesion assays and suggested by previous studies on the BSP-RGD domain (Gordon et al. 2009). In vivo observations showing reduced PDL at preeruption ages that progressed to increased PDL with deranged organization at later ages fit with this hypothesis. Additionally, caution is always warranted in use of in vitro mineralization assays, as they are subject to numerous variables (Bonewald et al. 2003), with cell density being relevant in functions of *Ibsp* knockout cells (Bouet et al. 2015).

In summary, we identified the BSP-RGD domain as a contributor to periodontal development and function. BSP-RGD has been implicated in osteoblast differentiation in vitro (Gordon et al. 2009), in line with other studies that point to the biological importance of RGD domains in a variety of proteins and contexts. These studies represent a first step toward understanding functions of BSP-RGD, with additional studies needed to expand beyond the limitations of animal numbers and to identify specific molecular functions in distinct cells and tissues.

## Author Contributions

K. Nagasaki, contributed to conception, design, data acquisition, analysis, and interpretation, drafted and critically revised the manuscript; M.B. Chavez, A. Nagasaki, contributed to conception,

design, data acquisition, analysis, and interpretation, critically revised the manuscript; J.M. Taylor, M.H. Tan, M. Ma, M.E. Thew, contributed to data acquisition and analysis, critically revised the manuscript; E. Ralston, contributed to data acquisition, analysis, and interpretation, critically revised the manuscript; D.-G. Kim, contributed to data analysis and interpretation, critically revised the manuscript; M.J. Somerman, B.L. Foster, contributed to conception, design, data analysis, and interpretation, critically revised the manuscript. All authors gave final approval and agree to be accountable for all aspects of the work.

## Acknowledgments

We thank Dr. Harvey Goldberg (Western University) and Dr. Larry Fisher (National Institute of Dental and Craniofacial Research/National Institutes of Health [NIH]) for discussions and provision of reagents for these studies, Dr. Chengyu Liu and Dr. Fan Zhang at the Transgenic Core Facility (National Heart, Lung, and Blood Institute/NIH) for their advice and generating the cell lines, and Dr. Davide Randazzo at the Light Imaging Section (National Institute of Arthritis and Musculoskeletal and Skin Diseases/National Institutes of Health) for slide scanning.

## Declaration of Conflicting Interests

The authors declared no potential conflicts of interest with respect to the research, authorship, and/or publication of this article.

## Funding

The authors disclosed receipt of the following financial support for the research, authorship, and/or publication of this article: This work was funded by the Japan Society for the Promotion of Science to A. Nagasaki (JSPS Research Fellowship for Japanese Biomedical and Behavioral Researchers at the National Institutes of Health); by the National Institute of Dental and Craniofacial Research/National Institutes of Health to support for M.B. Chavez (T32DE014320); by the National Institute of Dental and Craniofacial Research/National Institutes of Health to M.B. Chavez (F30DE030358); by the National Institute of Dental and Craniofacial Research/National Institutes of Health to B.L. Foster (R01DE027639); and by intramural funding from the National Institute of Arthritis and Musculoskeletal and Skin Diseases/National Institutes of Health to M.J. Somerman.

## ORCID iDs

K. Nagasaki https://orcid.org/0000-0003-0528-4025
A. Nagasaki https://orcid.org/0000-0002-7655-9658
B.L. Foster https://orcid.org/0000-0003-3444-0576

## References

Ao M, Chavez MB, Chu EY, Hemstreet KC, Yin Y, Yadav MC, Millan JL, Fisher LW, Goldberg HA, Somerman MJ, et al. 2017. Overlapping functions of bone sialoprotein and pyrophosphate regulators in directing cementogenesis. Bone. 105:134–147.

Bellahcène A, Bonjean K, Fohr B, Fedarko NS, Robey FA, Young MF, Fisher LW, Castronovo V. 2000. Bone sialoprotein mediates human endothelial cell attachment and migration and promotes angiogenesis. Circ Res. 86(8):885–891.

Bonewald LF, Harris SE, Rosser J, Dallas MR, Dallas SL, Camacho NP, Boyan B, Boskey A. 2003. von Kossa staining alone is not sufficient to confirm that mineralization in vitro represents bone formation. Calcif Tissue Int. 72(5):537–547.

Boudiffa M, Wade-Gueye NM, Guignandon A, Vanden-Bossche A, Sabido O, Aubin JE, Jurdic P, Vico L, Lafage-Proust MH, Malaval L. 2010. Bone sialoprotein deficiency impairs osteoclastogenesis and mineral resorption in vitro. J Bone Miner Res. 25(12):2669–2679.

Bouet G, Bouleftour W, Juignet L, Linossier MT, Thomas M, Vanden-Bossche A, Aubin JE, Vico L, Marchat D, Malaval L. 2015. The impairment of osteogenesis in bone sialoprotein (BSP) knockout calvaria cell cultures is cell density dependent. PLoS One. 10(2):e0117402.

Chavez MB, Chu EY, Kram V, de Castro LF, Somerman MJ, Foster BL. 2021. Guidelines for micro–computed tomography analysis of rodent dentoalveolar tissues. JBMR Plus. 5(3):e10474.

D'Errico JA, Ouyang H, Berry JE, MacNeil RL, Strayhorn C, Imperiale MJ, Harris NL, Goldberg H, Somerman MJ. 1999. Immortalized cementoblasts and periodontal ligament cells in culture. Bone. 25(1):39–47.

Fisher LW, Fedarko NS. 2003. Six genes expressed in bones and teeth encode the current members of the sibling family of proteins. Connect Tissue Res. 44 Suppl 1:33–40.

Foster BL, Ao M, Salmon CR, Chavez MB, Kolli TN, Tran AB, Chu EY, Kantovitz KR, Yadav M, Narisawa S, et al. 2018. Osteopontin regulates dentin and alveolar bone development and mineralization. Bone. 107:196–207.

Foster BL, Ao M, Willoughby C, Soenjaya Y, Holm E, Lukashova L, Tran AB, Wimer HF, Zerfas PM, Nociti FH Jr, et al. 2015. Mineralization defects in cementum and craniofacial bone from loss of bone sialoprotein. Bone. 78:150–164.

Foster BL, Soenjaya Y, Nociti FH Jr, Holm E, Zerfas PM, Wimer HF, Holdsworth DW, Aubin JE, Hunter GK, Goldberg HA, et al. 2013. Deficiency in acellular cementum and periodontal attachment in *Bsp* null mice. J Dent Res. 92(2):166–172.

Ganss B, Kim RH, Sodek J. 1999. Bone sialoprotein. Crit Rev Oral Biol Med. 10(1):79–98.

Goldberg HA, Warner KJ, Li MC, Hunter GK. 2001. Binding of bone sialoprotein, osteopontin and synthetic polypeptides to hydroxyapatite. Connect Tissue Res. 42(1):25–37.

Gordon JA, Hunter GK, Goldberg HA. 2009. Activation of the mitogen-activated protein kinase pathway by bone sialoprotein regulates osteoblast differentiation. Cells Tissues Organs. 189(1–4):138–143.

Holm E, Aubin JE, Hunter GK, Beier F, Goldberg HA. 2015. Loss of bone sialoprotein leads to impaired endochondral bone development and mineralization. Bone. 71:145–154.

Iwaniec UT, Yuan D, Power RA, Wronski TJ. 2006. Strain-dependent variations in the response of cancellous bone to ovariectomy in mice. J Bone Miner Res. 21(7):1068–1074.

Kajikawa T, Yamada S, Tauchi T, Awata T, Yamaba S, Fujihara C, Murakami S. 2014. Inhibitory effects of PLAP-1/asporin on periodontal ligament cells. J Dent Res. 93(4):400–405.

Karadag A, Fisher LW. 2006. Bone sialoprotein enhances migration of bone marrow stromal cells through matrices by bridging MMP-2 to v 3-integrin. J Bone Miner Res. 21(10):1627–1636.

Lee EH, Park HJ, Jeong JH, Kim YJ, Cha DW, Kwon DK, Lee SH, Cho JY. 2011. The role of asporin in mineralization of human dental pulp stem cells. J Cell Physiol. 226(6):1676–1682.

Liu L, Yu H, Long Y, You Z, Ogawa R, Du Y, Huang C. 2021. Asporin inhibits collagen matrix-mediated intercellular mechanocommunications between fibroblasts during keloid progression. FASEB J. 35(7):e21705.

MacNeil RL, Berry J, D'Errico J, Strayhorn C, Somerman MJ. 1995. Localization and expression of osteopontin in mineralized and nonmineralized tissues of the periodontium. Ann N Y Acad Sci. 760:166–176.

Malaval L, Wade-Gueye NM, Boudiffa M, Fei J, Zirngibl R, Chen F, Laroche N, Roux JP, Burt-Pichat B, Duboeuf F, et al. 2008. Bone sialoprotein plays a functional role in bone formation and osteoclastogenesis. J Exp Med. 205(5):1145–1153.

Mukhopadhyay P, Brock G, Webb C, Pisano MM, Greene RM. 2012. Strain-specific modifier genes governing craniofacial phenotypes. Birth Defects Res A Clin Mol Teratol. 94(3):162–175.

Naveh GRS, Foster JE, Santisteban TMS, Yang X, Olsen BR. 2018. Nonuniformity in ligaments is a structural strategy for optimizing functionality. Proc Natl Acad Sci U S A. 115(36):9008–9013.

Radlanski RJ, Renz H, Zimmermann CA, Mey R, Matalova E. 2015. Morphogenesis of the compartmentalizing bone around the molar primordia in the mouse mandible during dental developmental stages between lamina, bell-stage, and root formation (E13-P20). Ann Anat. 200:1–14.

Rapuano BE, Wu C, MacDonald DE. 2004. Osteoblast-like cell adhesion to bone sialoprotein peptides. J Orthop Res. 22(2):353–361.

Soenjaya Y, Foster BL, Nociti FH Jr, Ao M, Holdsworth DW, Hunter GK, Somerman MJ, Goldberg HA. 2015. Mechanical forces exacerbate periodontal defects in Bsp-null mice. J Dent Res. 94(9):1276–1285.

Tye CE, Hunter GK, Goldberg HA. 2005. Identification of the type I collagen-binding domain of bone sialoprotein and characterization of the mechanism of interaction. J Biol Chem. 280(14):13487–13492.

Valverde P, Tu Q, Chen J. 2005. BSP and RANKL induce osteoclastogenesis and bone resorption synergistically. J Bone Miner Res. 20(9):1669–1679.

Valverde P, Zhang J, Fix A, Zhu J, Ma W, Tu Q, Chen J. 2008. Overexpression of bone sialoprotein leads to an uncoupling of bone formation and bone resorption in mice. J Bone Miner Res. 23(11):1775–1788.

Wang L, Foster BL, Kram V, Nociti FH Jr, Zerfas PM, Tran AB, Young MF, Somerman MJ. 2014. Fibromodulin and biglycan modulate periodontium through TGFβ/BMP signaling. J Dent Res. 93(8):780–787.

Xu L, Li Z, Liu SY, Xu SY, Ni GX. 2015. Asporin and osteoarthritis. Osteoarthritis Cartilage. 23(6):933–939.

Xu L, Zhang Z, Sun X, Wang J, Xu W, Shi L, Lu J, Tang J, Liu J, Su X. 2017. Glycosylation status of bone sialoprotein and its role in mineralization. Exp Cell Res. 360(2):413–420.

Zhan S, Li J, Ge W. 2019. Multifaceted roles of asporin in cancer: current understanding. Front Oncol. 9:948.

Zhang H, Chavez MB, Kolli TN, Tan MH, Fong H, Chu EY, Li Y, Ren X, Watanabe K, Kim DG, et al. 2020. Dentoalveolar defects in the *Hyp* mouse model of X-linked hypophosphatemia. J Dent Res. 99(4):419–428.